

Reliable coherent optical memory based on a laser-written waveguide

CHAO LIU^{1,2}, ZONG-QUAN ZHOU^{1,2,*}, TIAN-XIANG ZHU^{1,2}, LIANG ZHENG^{1,2}, MING JIN^{1,2}, XIAO LIU^{1,2}, PEI-YUN LI^{1,2}, JIAN-YIN HUANG^{1,2}, YU MA^{1,2}, TAO TU^{1,2}, TIAN-SHU YANG^{1,2}, CHUAN-FENG LI^{1,2,†}, AND GUANG-CAN GUO^{1,2}

¹CAS Key Laboratory of Quantum Information, University of Science and Technology of China, Hefei 230026, People's Republic of China

²CAS Center For Excellence in Quantum Information and Quantum Physics, University of Science and Technology of China, Hefei 230026, People's Republic of China

*Corresponding author: zq_zhou@ustc.edu.cn

†Corresponding author: cfl@ustc.edu.cn

Compiled November 2, 2021

¹⁵¹Eu³⁺-doped yttrium silicate ($^{151}\text{Eu}^{3+} : \text{Y}_2\text{SiO}_5$) crystal is a unique material that possesses hyperfine states with coherence time up to 6 h. Many efforts have been devoted to the development of this material as optical quantum memories based on the bulk crystals, but integrable structures (such as optical waveguides) that can promote $^{151}\text{Eu}^{3+} : \text{Y}_2\text{SiO}_5$ -based quantum memories to practical applications, have not been demonstrated so far. Here we report the fabrication of type II waveguides in a $^{151}\text{Eu}^{3+} : \text{Y}_2\text{SiO}_5$ crystal using femtosecond-laser micromachining. The resulting waveguides are compatible with single-mode fibers and have the smallest insertion loss of 4.95 dB. On-demand light storage is demonstrated in a waveguide by employing the spin-wave atomic frequency comb (AFC) scheme and the revival of silenced echo (ROSE) scheme. We implement a series of interference experiments based on these two schemes to characterize the storage fidelity. Interference visibility of the readout pulse is 0.99 ± 0.03 for the spin-wave AFC scheme and 0.97 ± 0.02 for the ROSE scheme, demonstrating the reliability of the integrated optical memory. © 2021 Optical Society of America under the terms of the [OSA Open Access Publishing Agreement](#)

<https://doi.org/10.1364/OPTICA.379166>

1. INTRODUCTION

Optical quantum memories, which can map quantum information between light and matter with high fidelity, are crucial devices in the implementation for large-scale quantum networks[1][2]. As a promising candidate for this device, quantum memories with high fidelity [1][3][4], multi-mode capacity [4–7] as well as long storage time [8][9], have been demonstrated in bulk rare-earth-ion-doped crystals. To promote this remarkable device to practical application, many efforts have been devoted to the development of integrated quantum memories. Three approaches have been employed for manufacturing integrated quantum memories in rare-earth-ion-doped crystals. The first one is using industry-standard Ti indiffusion in

LiNbO₃. High fidelity [10][11], broadband [12][13], multiplexed [14] and telecom-wavelength [15] memory as well as integrated processor [16] have been demonstrated. The second one is using focused-ion-beam milling. Quantum memories with high fidelity [17] and telecom-wavelength [18] have also been demonstrated. However, the storage time and storage efficiencies in these two systems are significantly reduced as compared with that in bulk crystals [5][19][20]. As a result, spin-wave storage with extended lifetime have not been achieved based on these two approaches so far. The third one is using femtosecond-laser micromachining (FLM). Recently, integrable memories are successfully demonstrated, based on waveguides fabricated in a Pr³⁺ : Y₂SiO₅ crystal using FLM [21–23]. Storage time of up to 15 μs [21], storage efficiency as high as 21 % [22], and storage

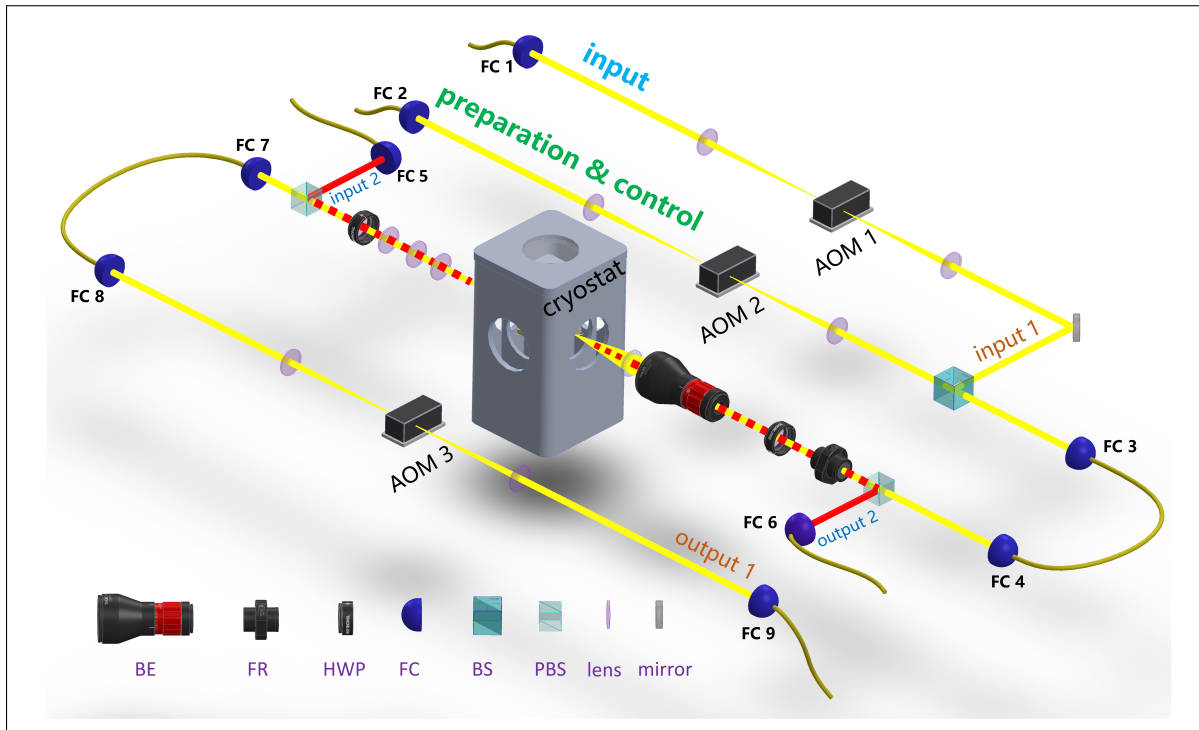


Fig. 1. Schematic of the experimental set up. The main laser beam is split into two to be employed as preparation & control mode and input mode respectively. The input mode can be injected through input 1 mode in the spin-wave AFC scheme or input 2 mode in the ROSE scheme. The yellow light beams represent optical paths for the spin-wave AFC memory scheme. The red beams denote the input and output mode for ROSE scheme. Labels at the left corner are: Beam Expander (BE), Faraday Rotator (FR), Half Wave Plate (HWP), Fiber Coupler (FC), Beam Splitter (BS), Polarizing Beam splitter (PBS), lens and mirror.

modes as many as 130 [23], have been achieved. These results are comparable with the performance of bulk crystals [24–26], thus making FLM an appealing technique to achieve integrated quantum memories. $^{151}\text{Eu}^{3+} : \text{Y}_2\text{SiO}_5$ crystal is an attractive candidate for optical quantum memories because of the longest storage time for single photons [8][9] and the longest spin coherence time [27] among the solid-state optical memories. However, there have been no demonstration of integrated memories in this material. More importantly, storage fidelity of the memory after fabrication using FLM has never been quantitatively characterized before, which is a critical figure-of-merit for coherent optical memories [28].

In this paper, we report the fabrication of the so-called type II waveguides [29] in a $^{151}\text{Eu}^{3+} : \text{Y}_2\text{SiO}_5$ crystal using FLM. Optimized fabrication parameters ensure that the waveguides are compatible with single-mode fibers (SMFs). On-demand light storage, based on the spin-wave atomic frequency comb (AFC) scheme [1][30] and the revival of silenced echo (ROSE) scheme [31], are demonstrated in the waveguide section, respectively. Then, storage fidelity of the memory after fabrication is characterized by performing a series of interference experiments based on these two schemes.

2. WAVEGUIDE FABRICATION

The substrate used here is an isotopically enriched $^{151}\text{Eu}^{3+} : \text{Y}_2\text{SiO}_5$ crystal (isotope enrichment of 99.9 %), with a dimension of $15 \times 5 \times 4$ mm ($b \times D_1 \times D_2$) and an ion concentration of 0.1 %. This crystal has the maximum absorption for the $^7F_0 \rightarrow ^5D_0$ transition at 580 nm when the light is polarized along the D_1 axis of the crystal. A FLM system

from WOPhotonics (Altechna R&D Ltd, Lithuania) is utilized to execute the fabrication. The femtosecond-laser beam, with a wavelength of 1030 nm, is injected along the D_2 axis. It is then focused 150 μm beneath the top face of the crystal with a $50\times$ objective ($NA = 0.65$). Two parallel damage tracks at a distance of 20 μm are formed by translating the crystal along the b axis with the speed of 575 $\mu\text{m}/\text{s}$ when the femtosecond-laser is shining. The fabrication parameters are: pulse duration of 300 fs, energy per pulse of 931 nJ, repetition rate of 201.9 kHz. We notice that these optimized fabrication parameters are largely different from that which are used to fabricate the same type of waveguides in $\text{Pr}^{3+} : \text{Y}_2\text{SiO}_5$ crystals [21][22].

The laser beam with wavelength of 580 nm can be effectively confined between these two tracks only when it is in horizontal polarization (parallel to the D_1 axis). This is compatible with the requirement of the efficient absorption for light in $\text{Eu}^{3+} : \text{Y}_2\text{SiO}_5$ crystals. Single-mode coupling efficiency of the laser beam when it's in horizontal polarization is typically 2 orders higher than that of in vertical polarization. This is consistent with previous work since type II waveguides usually support only one polarization mode [21][22][32]. We fabricate several waveguides in the same crystal and choose the most efficient one to perform the experiments, as different waveguides may have diverse coupling efficiencies even with the same fabrication parameters, owing to defects in the crystal.

3. EXPERIMENTAL SETUP

The laser source for the optical memory experiment is a frequency-doubled semiconductor laser (TA-SHG, toptica), which has an output power of 800 mW at a frequency of 516.848

THz. A high-stable cavity placed in a high-vacuum chamber is employed to lock the laser frequency, resulting in a line-width of sub-kHz. A cryostat (Montana Instrument) with the lowest working temperature of approximately 3.2 K is utilized to cool the sample. The sample is mounted on a 3-axis translator which has a positioning accuracy of 10 nm. All experiments are performed at low vibration time windows after synchronizing with the cycle of the cold head, which has a vibration period of approximately 700 ms. The total usable period for experiments is approximately 250 ms. As shown in Fig. 1, acoustic optic modulators (AOM) are employed to modulate the optical pulses. AOM 1 and AOM 2 are in double-pass configuration and are used to control the amplitude and frequency of each pulse. AOM 3 is in single-pass configuration and serves as an optical switch. Specifically, AOM 1 and AOM 3 are driven by an 8-channel arbitrary waveform generator (HDAWG, Zurich Instruments). Meanwhile, AOM 2 is driven by a modulated RF source, which can coherently control the phases of the optical pulses for heterodyne detections.

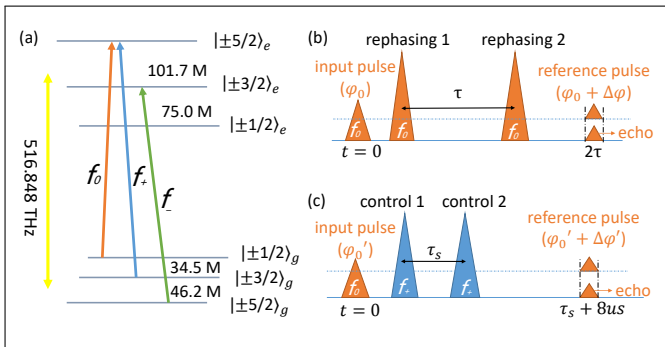


Fig. 2. (a) Energy level diagram of the ${}^7F_0 \rightarrow {}^5D_0$ transition of ${}^{151}\text{Eu}^{3+} : \text{Y}_2\text{SiO}_5$ at zero magnetic field. f_0 (orange), f_+ (blue) and f_- (green) denote optical transitions with different hyperfine levels. (b) Time sequence for the ROSE interference experiment. (c) Time sequence for the spin-wave AFC interference experiment. The triangles represent the optical pulses, while their frequencies are distinguished by the filled colors. The reference pulses are injected when the echoes come out. In the interference experiments, the time delays are fixed as $\tau = 4.94 \mu\text{s}$ for ROSE scheme and $\tau_s = 1.7 \mu\text{s}$ for spin-wave AFC scheme respectively.

For the spin-wave AFC scheme, input 1 and preparation & control beam are combined by a 92:8 beam splitter (BS). The combined light beam is expanded from a diameter of 2 mm to 6 mm by a beam expander (BE) and then focused at one end of the waveguide using a plano-convex lens ($f = 75 \text{ mm}$). This lens is also mounted on a 3-axis translator which has longer traveling distances. The focal spot has a diameter of $D = 5.4 \mu\text{m}$. This is calculated using the Gaussian beam focussing formula $D \approx \frac{2.36f\lambda}{\pi D_0}$. Here D_0 (6 mm) is the beam diameter before the plano-convex lens. Under the help of a long working distance microscope above the cryostat, strong red fluorescence can be observed when the laser beam passes through the crystal and resonates with the ${}^{151}\text{Eu}^{3+}$ ions. By carefully adjusting the two 3-axis stage, the red fluorescence can be almost completely confined between the two damage tracks. Output laser beam after the waveguide is collected by a fiber coupler (FC 7) after three lenses of different focal lengths, and then is sent to a photo detector or a photo multiplier tube (PMT) after passing the optical

switch (AOM 3).

The optimized coupling efficiency into the SMF is 24 %, which is calculated as the ratio between the power of the output beam after FC 7 and input power before the cryostat. Considering the transmission efficiency of 75 % for other optical elements, insertion loss of the waveguide can be calculated as 4.95 dB. We notice that the insertion loss here is approximately half of that has been achieved in industry-standard waveguides [12][13][15]. For the ROSE scheme, the preparation & control mode is the same as the spin-wave AFC scheme. However, the input 2 mode is injected from FC 5 and then collected by FC 6. Thus the input mode and control mode are in counter-propagating configuration, to silent the standard photon echo using phase mismatching [31].

4. RESULTS

A. SAMPLE CHARACTERIZATION

Spectral preparation is the prerequisite for the implementation of optical memory. This is achieved by two steps based on spectral hole burning technique [33]. The first step named class cleaning. Preparation pulses with center frequency of f_0 , $f_+(= f_0 + 34.5 \text{ MHz})$ and $f_-(= f_0 - 20.9 \text{ MHz})$ are applied simultaneously. The preparation pulses last for 2 ms and repeat for 100 times. After this process, one class ions is picked up and other classes ions are all pumped away. The second step is called spin polarization. This step is done by applying preparation pulses with center frequency of f_+ and f_- and repeating them for 100 times. During these two steps, each frequency is swept over 4 MHz. Finally, the ions are polarized to $|\pm 1/2\rangle_g$ over this frequency range.

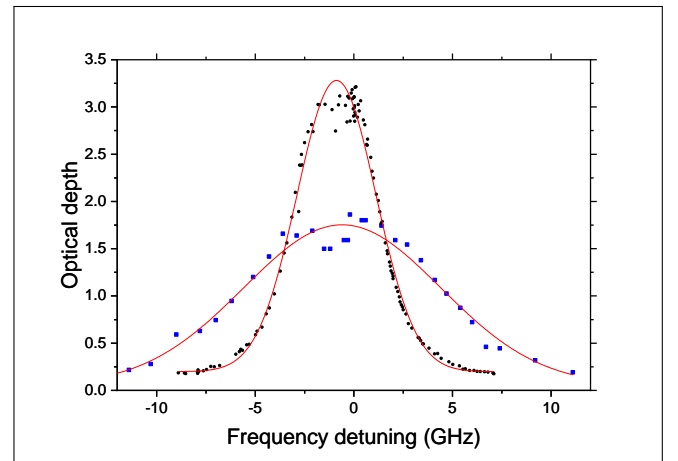


Fig. 3. Absorption profile of the sample. Black dots are experimental data collected in the bulk section, while the experimental data in the waveguide are represented in blue squares. Gaussian fitting gives the optical inhomogeneous broadening $\Gamma_{inh}(FWHM)$: 4.7 GHz in the bulk section and 11.8 GHz in the waveguide. Zero detuning corresponds to 516.848 THz.

The input pulse is a Gaussian pulse with frequency of f_0 and full width at half maximum (FWHM) duration of approximately 500 ns. The intensity (P_a) of the transmission pulse is recorded by a photon detector (Thorlabs, PDA8A). The intensity of the input pulse (P_0) is obtained by burning a transparent window at f_0 . In the waveguide section, P_a/P_0 is measured to be 17.4 %. It

corresponds to an OD of 1.75. In contrast, an OD of 3.00 is measured in the bulk crystal. The reduction of OD can be explained by the expansion of the optical inhomogeneous broadening in the waveguide after fabrication, which is broadened by more than 2 times compared with that of in the bulk section (see fig. 3).

The optical coherence time T_2 is measured by performing a series of two-pulse photon echo experiments. The first input pulse, with a duration (FWHM) of 500 ns, is injected at $t = 0$, generating a superposition state between $|\pm 1/2\rangle_g$ and $|\pm 5/2\rangle_e$. Then, a refocusing pulse is injected at $t = \tau_1$ and a photon echo is induced at $t = 2\tau_1$. Due to smaller amount ions involved during the whole process, the photon echo is small and is not easy to be detected by a photon detector when τ_1 is larger than 10 μs . So a heterodyne detection is employed here to obtain the echo amplitude. T_2 is extracted from the exponential decay of echo amplitude as τ_1 increases (shown in Fig. 4). The peak power of the input pulse is 0.5 mW in the waveguide section. The fitted $T_2 = 202 \pm 3 \mu\text{s}$. As a comparison, the peak power is approximately 5.3 mW in the bulk section. The fitted $T_2 = 186 \pm 7 \mu\text{s}$. This result indicates that the coherence property of the memory is not affected during the fabrication process.

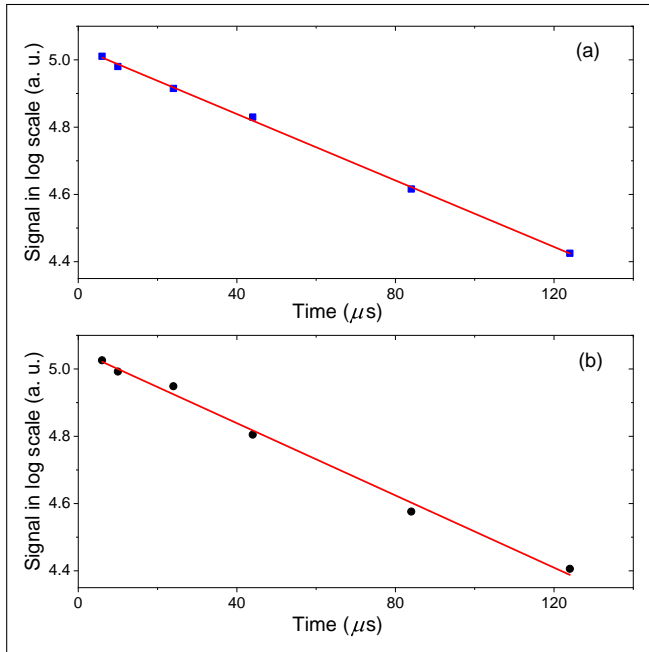


Fig. 4. Photon echo amplitude (in logarithmic scale) as a function of time spacing between the two pulses. (a) Measurement performed in the waveguide section. Linear fitting gives $T_2 = 202 \pm 3 \mu\text{s}$. (b) Measurement performed in the bulk section. Linear fitting gives $T_2 = 186 \pm 7 \mu\text{s}$.

B. ROSE STORAGE

The ROSE scheme is free from the noise induced by the inversion of medium population in the conventional two-pulse photon echo scheme [34], thus has the potential to demonstrate optical storage at the single-photon level [31][35]. In ROSE scheme, a second rephasing pulse is applied to bring the atoms excited by the first rephasing pulse back to the ground state, and to reverse the phases of them, leading to a secondary echo. The primary echo is silenced when spatial phase mismatching is fulfilled such

as the counter-propagating configuration used here.

To benchmark the memory performance in terms of the coherent storage, here we implement an interference experiment to characterize the storage fidelity [28][36][37]. The experimental time sequence is shown in Fig. 2 (b). The input pulse is the same as that utilized in the measurements of absorption and T_2 . Then two rephasing pulses (also at frequency f_0) with spacing of τ are injected, resulting in a ROSE echo at 2τ . Complex hyperbolic secant (CHS) pulses [38][39] are utilized here as the rephasing pulses. They have a duration of 0.94 μs and a peak power of 13 mW (before the cryostat). A Gaussian reference pulse with relative phase of $\Delta\varphi$ to the first input pulse is injected at 2τ , to interfere with the echo. Careful alignments are made to ensure temporal overlap between the echo and the reference pulse. The output signals are measured by the photon detector and displayed on an oscilloscope. We read the peak value of each interference pattern to form the final interference curve. Fig. 5 (a) shows the interference curve with a fixed τ (4.94 μs) when $\Delta\varphi$ increases 20 degrees step by step. Intensity of the interference signal can be represented by:

$$I(\varphi) = \frac{I_{max}}{2} [1 + V \sin(\varphi + \varphi_1)], \quad (1)$$

where I_{max} is the maximum signal intensity, φ is the relative

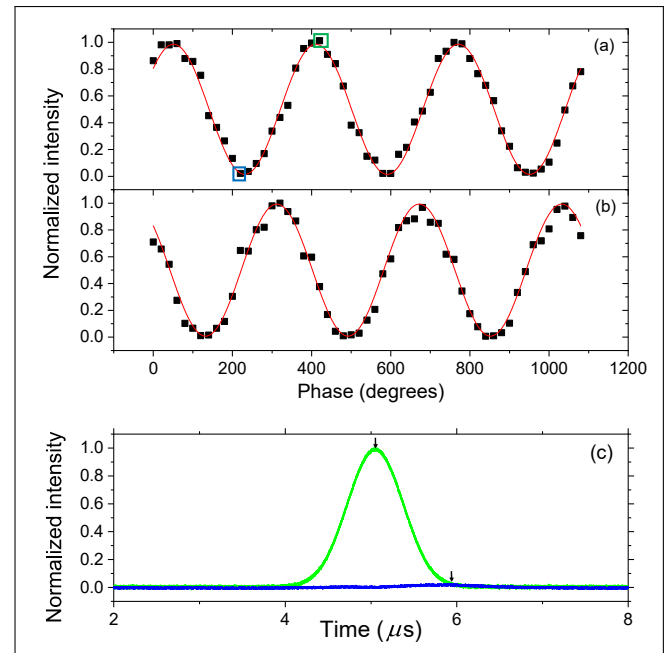


Fig. 5. Normalized intensity of the output light as a function of the relative phases between the input pulse and reference pulse. Interference visibilities are fitted by using Eq (1). (a) For the ROSE scheme, $V = 0.97 \pm 0.02$. (b) For the spin-wave AFC scheme, $V = 0.99 \pm 0.03$. (c) Examples of interference patterns for ROSE scheme. Blue lines corresponds to data marked with blue square and green lines corresponds to data marked with green square in Fig. 5(a). Black arrows indicate the peak positions. The peak of the blue curve is away from the original pulse center because of the imperfect interference in the tail of the pulse.

phase between the input pulse and reference pulse, φ_1 is the phase offset, V is the interference visibility. The interference

curve is well fitted by this formula with $V = 0.97 \pm 0.02$, indicating that the relative phases are well preserved during the whole storage process.

Considering the finite transfer efficiency of the rephasing pulses, the storage efficiency can be expressed as [31]:

$$\eta = \eta_T^2 (OD)^2 e^{-OD} e^{-4\tau/T_{2eff}}, \quad (2)$$

η_T denotes the transfer efficiency of a single rephasing pulse, T_{2eff} is the effective coherence time. Fig. 6 (a) shows the storage efficiency as a function of the storage time. The fitted $T_{2eff} = 37.4 \pm 0.9 \mu\text{s}$, is obviously shorter than the optical coherence time. This is attributed to the severe instantaneous spectral diffusion (ISD) effect [22][40][41] induced by the massive rephasing pulses. A possible way to minimize this effect is reducing the storage bandwidth [41]. Moreover, longer storage time can be expected by transferring the coherence to spin states [42]. The maximally possible storage efficiency is extracted as $\eta_0 = 34.4 \%$ when $\tau = 0$. η_T is then deduced as 80 %.

C. SPIN-WAVE AFC STORAGE

The AFC scheme is based on spectral shaping of an inhomogeneously broadened optical transition [30]. By applying spectral hole burning sequences, a comb with periodicity of Δ can be shaped. When a photon is injected, it will be absorbed by the comb. Its state is mapped into a collective excitation of the atoms that resonate with the photon, and can be written as a collective Dicke state: $\sum_j e^{-i2\pi\delta_j t} |g_1 \dots e_j \dots g_N\rangle$, $\delta_j = m_j \Delta$ (m_j is an integer number) is the frequency detuning of the atom j [22][30]. The atoms will dephase since different atom will acquire a different phase ($e^{i\delta_j t}$) after a period of t . However, after a predetermined time $\frac{1}{\Delta}$, they will collectively rephase, leading to a photon re-emission. In order to achieve long storage time and on-demand readout, a pair of control pulses can be applied to transfer the collective excitation in and out another ground spin state. This is the so-called spin-wave AFC storage.

After finishing class cleaning and spin polarization, comb on $|\pm 1/2\rangle_g \rightarrow |\pm 5/2\rangle_e$ transition can be created. Here we employ the parallel preparation sequence [43] to create all absorption teeth in parallel. We prepare an AFC with bandwidth of 2 MHz and a two-level storage time of 8 μs . The preparation pulse has a duration of 2 ms and is repeated for 50 times to create a high quality comb. The time sequence for AFC storage is shown in Fig. 2. (c). The input pulse is same as previous and is injected at $t = 0$. The AFC echo comes out at $t = 8 \mu\text{s}$, and the corresponding storage efficiency is 5 %. In order to realize spin-wave AFC storage, two control pulses with the center frequency of f_+ and a chirp bandwidth of 2 MHz after the input pulse are injected. They have a duration of 1.7 μs and a peak power of 11 mW before the cryostat. The pulse spacing between them is τ_s . The spin-wave AFC echo comes out at $\tau_s + 8 \mu\text{s}$ and its intensity is decreased by approximately an order compared with the AFC echo. The fast dephasing on the spin state is the primary source for the reduction of efficiency. As shown in Fig. 6 (b), $T_2^* = 3.3 \pm 0.2 \mu\text{s}$. The inhomogeneous spin line-width (γ_{inh}) is deduced as 114 kHz, using the formula $\gamma_{inh} = \frac{\sqrt{2}m_2/\pi}{T_2^*}$ [44][45]. As a comparison, the inhomogeneous spin line-width is 60 kHz in the bulk, measured by Raman-Heterodyne technique. This broadening magnitude is compatible with that of the optical inhomogeneous broadening.

In order to verify the fidelity of the spin-wave AFC memory, a reference pulse with a relative phase of $\Delta\phi'$ to input pulse is

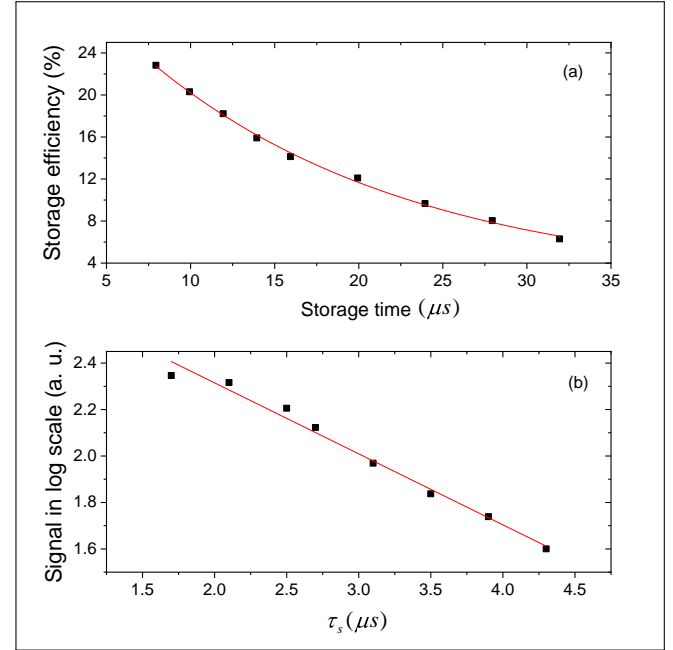


Fig. 6. (a) Storage efficiency as a function of storage time for the ROSE scheme. The maximum storage efficiency is deduced as $\eta_0 = 34.4 \%$ at $\tau = 0$, and the extracted effective coherence time is $T_{2eff} = 37.4 \pm 0.9 \mu\text{s}$. (b) Spin-wave AFC echo amplitude as a function of τ_s . τ_s denotes the pulse spacing between the two control pulses, which is the spin-wave storage time. T_2^* is fitted as $3.3 \pm 0.2 \mu\text{s}$.

injected at $t = 9.7 \mu\text{s}$ (τ_s is fixed as 1.7 μs) to interfere with the spin-wave AFC echo. The relative phase increases with a step of 20 degrees. The intensities of the output signals are recorded by a PMT. Usually, the PMT has a very nonlinear response to the intensity of the input pulse (see supplementary material for detail), data shown in Fig. 5 (b) are calibrated and normalized. The processes on interference patterns are similar with the ROSE scheme. The interference visibility of $V = 0.99 \pm 0.03$ is obtained, revealing the phase-preserving property of the the spin-wave AFC memory.

5. DISCUSSION AND CONCLUSION

In conclusion, SMF-compatible waveguides in a $^{151}\text{Eu}^{3+}:\text{Y}_2\text{SiO}_5$ crystal are fabricated using FLM. On-demand light storage is demonstrated in a waveguide based on the spin-wave AFC and ROSE scheme. The reliability of waveguide-based optical memory is demonstrated by performing a series of interference experiments based on these two schemes with almost unit visibility. In our current waveguide configuration, the free induction decay is the main source of noise for both memory schemes. This kind of noise can be rejected by utilizing polarization filtering based on other types of waveguides which support more than one polarization mode [29].

Also, we notice that the fabrication process causes absorption reduction and fast dephasing on spin states, which are unfavorable for optical quantum memory schemes, especially for the spin-wave AFC scheme. The first problem is attributed to the expansion of the optical inhomogeneous broadening after fabrication, and can be solved by using a longer crystal or increasing

the dopant concentration. The second problem is obviously correlated with the optical inhomogeneous broadening, in view of similar magnitude of broadening after fabrication. The fabrication parameters should be further optimized to find a trade-off between the single-mode coupling efficiency (preferring severer damage) and the line-width broadening (preferring weaker damage). We note that the storage time can be further extended with the help of a carefully aligned magnetic field [27][46] and the dynamical decoupling sequences [8] [28], to fulfill the requirements for long-distance entanglement distribution [2].

FUNDING INFORMATION

This work was supported by the National Key R&D Program of China (No. 2017YFA0304100), the National Natural Science Foundation of China (Nos. 11774331, 11774335, 11504362, 11821404, 11654002), Anhui Initiative in Quantum Information Technologies (No. AHY020100), Key Research Program of Frontier Sciences, CAS (No. QYZDY-SSW-SLH003), Science Foundation of the CAS (No. ZDRW-XH-2019-1), the Fundamental Research Funds for the Central Universities (No. WK2470000026).

ACKNOWLEDGMENTS

The authors thanks the technical help from Titas Gertus and Orestas Ulcinas.

DISCLOSURES

Disclosures. The authors declare no conflicts of interest.

SUPPLEMENTAL DOCUMENTS

Please see Supplementary material for supporting content.

REFERENCES

1. H. de Riedmatten, M. Afzelius, M. U. Staudt, C. Simon, and N. Gisin, "A solid-state light-matter interface at the single-photon level," *Nature* **456**, 773–777 (2008).
2. N. Sangouard, C. Simon, H. de Riedmatten, and N. Gisin, "Quantum repeaters based on atomic ensembles and linear optics," *REVIEW OF MODERN PHYSICS* **83**, 33–80 (2011).
3. Z. Q. Zhou, W. B. Lin, M. Yang, C. F. Li, and G. C. Guo, "Realization of reliable solid-state quantum memory for photonic polarization qubit," *Phys. Rev. Lett.* **108**, 190505 (2012).
4. Z. Q. Zhou, Y. L. Hua, X. Liu, G. Chen, J. S. Xu, Y. J. Han, C. F. Li, and G. C. Guo, "Quantum storage of three-dimensional orbital-angular-momentum entanglement in a crystal," *Phys. Rev. Lett.* **115**, 070502 (2015).
5. I. Usmani, M. Afzelius, H. D. Riedmatten, and N. Gisin, "Mapping multiple photonic qubits into and out of one solid-state atomic ensemble," *Nat. Commun.* **1**, 12 (2010).
6. J. S. Tang, Z. Q. Zhou, Y. T. Wang, Y. L. Li, X. Liu, Y. L. Hua, Y. Zou, S. Wang, D. Y. He, G. Chen, Y. N. Sun, Y. Yu, M. F. Li, G. W. Zha, H. Q. Ni, Z. C. Niu, C. F. Li, and G. C. Guo, "Storage of multiple single-photon pulses emitted from a quantum dot in a solid-state quantum memory," *Nat. Commun.* **6**, 8652 (2015).
7. T.-S. Yang, Z.-Q. Zhou, Y.-L. Hua, X. Liu, Z.-F. Li, P.-Y. Li, Y. Ma, C. Liu, P.-J. Liang, X. Li, Y.-X. Xiao, J. Hu, C.-F. Li, and G.-C. Guo, "Multiplexed storage and real-time manipulation based on a multiple degree-of-freedom quantum memory," *Nat. Commun.* **9**, 3407 (2018).
8. P. Jobez, C. Laplane, N. Timoney, N. Gisin, A. Ferrier, P. Goldner, and M. Afzelius, "Coherent spin control at the quantum level in an ensemble-based optical memory," *Phys. Rev. Lett.* **114**, 230502 (2015).
9. C. Laplane, P. Jobez, J. Etesse, N. Gisin, and M. Afzelius, "Multimode and long-lived quantum correlations between photons and spins in a crystal," *Phys. Rev. Lett.* **118**, 210501 (2017).
10. M. U. Staudt, S. R. Hastings-Simon, M. Nilsson, M. Afzelius, V. Scarani, R. Ricken, H. Suche, W. Sohler, W. Tittel, and N. Gisin, "Fidelity of an optical memory based on stimulated photon echoes," *Phys. Rev. Lett.* **98**, 113601 (2007).
11. M. U. Staudt, M. Afzelius, H. de Riedmatten, S. R. Hastings-Simon, C. Simon, R. Ricken, H. Suche, W. Sohler, and N. Gisin, "Interference of multimode photon echoes generated in spatially separated solid-state atomic ensembles," *Phys Rev Lett* **99**, 173602 (2007).
12. N. Sinclair, D. Oblak, C. W. Thiel, R. L. Cone, and W. Tittel, "Properties of a rare-earth-ion-doped waveguide at subkelvin temperatures for quantum signal processing," *Phys. Rev. Lett.* **118**, 100504 (2017).
13. E. Saglamyurek, N. Sinclair, J. Jin, J. A. Slater, D. Oblak, F. Bussières, M. George, R. Ricken, W. Sohler, and W. Tittel, "Broadband waveguide quantum memory for entangled photons," *Nature*. **469**, 512–515 (2011).
14. N. Sinclair, E. Saglamyurek, H. Mallahzadeh, J. A. Slater, M. George, R. Ricken, M. P. Hedges, D. Oblak, C. Simon, W. Sohler, and W. Tittel, "Spectral multiplexing for scalable quantum photonics using an atomic frequency comb quantum memory and feed-forward control," *Phys Rev Lett* **113**, 053603 (2014).
15. M. F. Askarani, M. G. Puigibert, T. Lutz, V. B. Verma, M. D. Shaw, S. W. Nam, N. Sinclair, D. Oblak, and W. Tittel, "Storage and reemission of heralded telecommunication-wavelength photons using a crystal waveguide," *Phys. Rev. Appl.* **11**, 054056 (2019).
16. E. Saglamyurek, N. Sinclair, J. A. Slater, K. Heshami, D. Oblak, and W. Tittel, "An integrated processor for photonic quantum states using a broadband light-matter interface," *New J. Phys.* **16**, 065019 (2014).
17. T. Zhong, J. M. Kindem, J. G. Bartholomew, J. Rochman, I. Craiciu, E. Miyazono, M. Bettinelli, E. Cavalli, V. Verma, S. W. Nam, F. Marsili, M. D. Shaw, A. D. Beyer, and A. Faraon, "Nanophotonic rare-earth quantum memory with optically controlled retrieval," *Science*. **357**, 1392 (2017).
18. I. Craiciu, M. Lei, J. Rochman, J. M. Kindem, J. G. Bartholomew, E. Miyazono, T. Zhong, N. Sinclair, and A. Faraon, "Nanophotonic quantum storage at telecommunication wavelength," *Phys. Rev. Appl.* **12**, 024062 (2019).
19. T. Chaneliere, M. Bonarota, V. Damon, R. Lauro, J. Ruggiero, I. Lorgere, and J. L. L. Gouet, "Light storage protocols in tm:ya₃," *J. Lumin.* **130**, 1572–1578 (2010).
20. B. Lauritzen, J. c. v. Minář, H. de Riedmatten, M. Afzelius, N. Sangouard, C. Simon, and N. Gisin, "Telecommunication-wavelength solid-state memory at the single photon level," *Phys. Rev. Lett.* **104**, 080502 (2010).
21. G. Corrielli, A. Seri, M. Mazzera, R. Osellame, and H. D. Riedmatten, "Integrated optical memory based on laser-written waveguides," *Phys. Rev. Appl.* **5**, 054013 (2016).
22. A. Seri, G. Corrielli, D. Lago-Rivera, A. Lenhard, H. de Riedmatten, R. Osellame, and M. Mazzera, "Laser-written in-

- egrated platform for quantum storage of heralded single photons," *Optica*, **5**, 934–941 (2018).
23. A. Seri, D. Lago-Rivera, A. Lenhard, G. Corrielli, R. Osellame, M. Mazzer, and H. de Riedmatten, "Quantum storage of frequency-multiplexed heralded single photons," *Phys. Rev. Lett.* **123**, 080502 (2019).
 24. K. Kutluer, M. Mazzer, and H. de Riedmatten, "Solid-state source of nonclassical photon pairs with embedded multimode quantum memory," *Phys. Rev. Lett.* **118**, 210502 (2017).
 25. M. Afzelius, I. Usmani, A. Amari, B. Lauritzen, A. Walther, C. Simon, N. Sangouard, J. C. v. Minář, H. de Riedmatten, N. Gisin, and S. Kröll, "Demonstration of atomic frequency comb memory for light with spin-wave storage," *Phys. Rev. Lett.* **104**, 040503 (2010).
 26. M. Gündoğan, P. M. Ledingham, K. Kutluer, M. Mazzer, and H. de Riedmatten, "Solid state spin-wave quantum memory for time-bin qubits," *Phys. Rev. Lett.* **114**, 230501 (2015).
 27. M. Zhong, M. P. Hedges, R. L. Ahlefeldt, J. G. Bartholomew, S. E. Beavan, S. M. Wittig, J. J. Longdell, and M. J. Sellars, "Optically addressable nuclear spins in a solid with a six-hour coherence time," *Nature*, **517**, 177 (2015).
 28. M. Lovrić, D. Suter, A. Ferrier, and P. Goldner, "Faithful solid state optical memory with dynamically decoupled spin wave storage," *Phys. Rev. Lett.* **111**, 020503 (2013).
 29. F. Chen and J. R. V. de Aldana, "Optical waveguides in crystalline dielectric materials produced by femtosecond-laser micromachining," *Laser Photonics Rev.* **8**, 251–275 (2014).
 30. M. Afzelius, C. Simon, H. D. Riedmatten, and N. Gisin, "Multimode quantum memory based on atomic frequency combs," *Phys. Rev. A - At. Mol. Opt. Phys.* **79**, 052329 (2009).
 31. V. Damon, M. Bonarota, A. Louchet-Chauvet, T. Chanelière, and J. L. L. Gouët, "Revival of silenced echo and quantum memory for light," *New J. Phys.* **13**, 093031 (2011).
 32. J. Siebenmorgen, K. Petermann, G. Huber, K. Rademaker, S. Nolte, and A. Tünnermann, "Femtosecond laser written stress-induced $\text{nd}:\text{y}_3\text{al}_5\text{o}_{12}$ ($\text{nd}:\text{yag}$) channel waveguide laser," *Appl. Phys. B: Lasers Opt.* **97**, 251–255 (2009).
 33. B. Lauritzen, N. Timoney, N. Gisin, M. Afzelius, H. de Riedmatten, Y. Sun, R. M. Macfarlane, and R. L. Cone, "Spectroscopic investigations of $\text{eu}^{3+}:\text{y}_2\text{seo}_5$ for quantum memory applications," *Phys. Rev. B* **85**, 115111 (2012).
 34. N. A. Kurnit, I. D. Abella, and S. R. Hartmann, "Observation of a photon echo," *Phys. Rev. Lett.* **13**, 567–568 (1964).
 35. M. Bonarota, J. Dajczgiewand, A. Louchet-Chauvet, J. L. L. Gouët, and T. Chanelière, "Photon echo with a few photons in two-level atoms," *Laser Phys* **24** (2014).
 36. K. F. Reim, J. Nunn, V. O. Lorenz, B. J. Sussman, K. C. Lee, N. K. Langford, D. Jaksch, and I. A. Walmsley, "Towards high-speed optical quantum memories," *Nat. Photonics* **4**, 218–221 (2010).
 37. Y.-H. Chen, M.-J. Lee, I. C. Wang, S. Du, Y.-F. Chen, Y.-C. Chen, and I. A. Yu, "Coherent optical memory with high storage efficiency and large fractional delay," *Phys. Rev. Lett.* **110**, 083601 (2013).
 38. M. S. Silver, R. I. Joseph, and D. I. Hoult, "Selective spin inversion in nuclear magnetic resonance and coherent optics through an exact solution of the bloch-riccati equation," *Phys Rev A Gen Phys* **31**, 2753–2755 (1985).
 39. L. Rippe, M. Nilsson, S. Kröll, R. Klieber, and D. Suter, "Experimental demonstration of efficient and selective population transfer and qubit distillation in a rare-earth-metal-ion-doped crystal," *Phys. Rev. A - At. Mol. Opt. Phys.* **71**, 062328 (2005).
 40. J. R. Klauder and P. W. Anderson, "Spectral diffusion decay in spin resonance experiments," *Phys. Rev.* **125**, 912–932 (1962).
 41. J. Dajczgiewand, R. Ahlefeldt, T. Böttger, A. Louchet-Chauvet, J.-L. L. Gouët, and T. Chanelière, "Optical memory bandwidth and multiplexing capacity in the erbium telecommunication window," *New J. Phys.* **17**, 023031 (2015).
 42. G. Demeter, "Coherence rephasing combined with spin-wave storage using chirped control pulses," *Phys. Rev. A* **89**, 063806 (2014).
 43. P. Jobez, N. Timoney, C. Laplane, J. Etesse, A. Ferrier, P. Goldner, N. Gisin, and M. Afzelius, "Towards highly multimode optical quantum memory for quantum repeaters," *Phys. Rev. A* **93**, 032327 (2016).
 44. M. Gündoğan, M. Mazzer, P. M. Ledingham, M. Cristiani, and H. de Riedmatten, "Coherent storage of temporally multimode light using a spin-wave atomic frequency comb memory," *New J. Phys.* **15**, 045012 (2013).
 45. N. Timoney, B. Lauritzen, I. Usmani, M. Afzelius, and N. Gisin, "Atomic frequency comb memory with spin-wave storage in $\text{eu}^{3+}:\text{y}_2\text{seo}_5$," *J. Phys. B: At. Mol. Opt. Phys.* **45**, 124001 (2012).
 46. C. Langer, R. Ozeri, J. D. Jost, J. Chiaverini, B. DeMarco, A. Ben-Kish, R. B. Blakestad, J. Britton, D. B. Hume, W. M. Itano, D. Leibfried, R. Reichle, T. Rosenband, T. Schaetz, P. O. Schmidt, and D. J. Wineland, "Long-lived qubit memory using atomic ions," *Phys. Rev. Lett.* **95**, 060502 (2005).